Modulations of face perception in response to a novel time-varying optical perturbation after aberration correction using adaptive optics

Elie de Lestrange-Anginieur[1,2,*], Yichen Ding[3,*]

[1] School of Optometry, The Hong Kong Polytechnic University, Hong Kong, China

[2] Applied Optics Group, Department of Experimental Physics, National University of Ireland, Galway, H91 CF50, Ireland

[3] Department of Bioengineering, Erik Jonsson School of Engineering and Computer Science, The University of Texas at Dallas, Richardson, TX 75080, USA

Abstract. The role of time in the perception of optical perturbation has received little attention. We sought to establish a novel time-varying perturbation in an image sequence using adaptive optics. We introduced the interpolated blur as a probe of visual processing, including four originally identical image frames whose position and pattern were manipulated to transform the time-averaged aberration. The resulting effects of interpolated blur were measured by comparing the dynamic sequence with the reference stimulus under the same condition of time-averaged aberration. Our results demonstrated that the perception of the time-averaged aberration depends on the optical perturbation, suggesting the potential modulations of interpolated blur on the correction of spatial blur. Our findings provide an entry point to implement adaptive optical correction to investigate dynamic changes of interpolated blurs.

Keywords: interpolated blur, time-averaged aberration, adaptive optics, human faces.

*Correspondence:

Elie de Lestrange-Anginieur, Ph.D.

elie.delestrange@hotmail.com

Yichen Ding, Ph.D.

Yichen.Ding@utdallas.edu

1. Introduction

At every instant, our retina is bombarded by rapidly-varying visual information competing for processing, but only limited information can be processed at once by the visual system [1]. The extent of visual processing is ascribed to both optical quality of the retinal stimulus and neural filtering [2], which constrained spatial resolution and quality. When an image is perfectly focused, visual rendering is principally dependent on the temporal deployment of the neural response acting through two main visual channels [3-5]: a transient channel associated with the fast magnocellular neurons that favors low spatial frequency, and a sustained channel with the slower parvo cellular neurons that favors high spatial frequencies [6, 7]. Owing to the distinct spatiotemporal sensitivity and responses of these pathways, the neural filter could flexibly tune to a retinal stimulus continuously varied by the oculomotor and stimulus dynamics. In fact, several studies evidenced a variation of processing over time [8], with a prevalent temporal precedence of low spatial frequency [9]. However, the effects on neural filtering of the balance between low and high spatial frequency constrained by the ocular aberrations remain elusive.

In this respect, studies examining the impact of ocular aberrations in vision enhancement highlighted a predominant impact of optical quality over neural filtering [10-15]. The use of simple and static stimulus with long exposure is insufficient to reveal the complex temporal interactions shaping neural filtering over time, regardless of rapid and unpredictable temporal changes. It has been recently shown that modulation in neural processing differentially affect corrected and aberrated images [16, 17], suggesting that aberrations could lead to differences in neural filtering. While a few studies tried to unveil the neural code associated to ocular aberrations [18, 19], the influence of images processed over time under variable ocular aberrations are to be defined. Predicting the processed information at different instant enables to enhance visual rendering (e.g.

the match between optical inputs and neural outputs over time), reducing the detection of irrelevant information susceptible to compete for processing.

In this study, we sought to examine how neural filtering varies with ocular aberrations over time. We developed a novel time-varying optical perturbation technique, where a blurred frame interpolated in an image sequence was used as a probe of visual processing to reveal whether the perturbation was effectively detected at a given time. This interpolated blur, consisting of either a rotational or directional blurred pattern, randomly appeared at different temporal positions of a fifteen-frame sequence with a fixed temporal frequency of 7.5 Hz and introduced an abrupt spatial variation called optical perturbation in the image sequence. The visual effect of this perturbation was evaluated by asking subjects to compare a dynamic stimulus including the interpolated blur, and a static sequence sharing same contrast across spatial frequencies in average over time.

Previous studies looking at the temporal information detected by the visual system over time using a time-varying perturbation did not control the effect of the ocular aberrations remodeling the spatial scale and orientations of the retinal image[20,21]. Our hypothesis was that the sensitivity of a neural filter at different times depends on the retinal image quality set by the aberrations of the eye. To test the hypothesis, we used an adaptive optics visual analyzer to correct the ocular aberrations of different subjects, ensuring that images were presented in individual eyes under the same condition over time. Concurrently with the adaptive optics correction, the dynamic and static image sequences were digitally filtered using computer-generated aberration. Static and dynamic sequence were blurred with the same time-averaged aberration that simulated the retinal image viewed with ocular aberrations in absence of the temporal changes produced by the oculomotor dynamics (blinks, pupillary movement, etc.). However, whereas the same blur was applied on each frame of the static sequence, a temporal change was introduced by the interpolated blur inserted in the dynamic sequence.

We implemented three independent experiments to investigate whether ocular aberrations impel a different sensitivity to interpolated blurs. In the first experiment, subjects were asked to identify and classify the transformation of a dynamic face sequence associated with the magnitude of the interpolated blur, in comparison to a reference static face sequence. In the second experiment, subjects were instructed to compare the sharpness of the dynamic and static face sequences. In the last experiment, subjects were requested to discriminate the difference of the face expression of a dynamic and static face sequence. Our results indicate that interpolated blurs differentially affect the perception of images viewed with and without aberration, demonstrating that optical perturbation affects neural filtering over time.

2. Results

2.1 Experimental conditions

To test the influence of common imperfections of the ocular system on temporal processing, the time-averaged face stimuli of the static and dynamic sequence were viewed under three types of optical viewing conditions, as follows:

(i) the time-averaged diffraction-limited condition DL_{avg}, which simulates an eye free from optical imperfections.

(ii) the time-averaged native aberration NA_{avg}, which simulates the natural ocular aberrations for each subject's eye tested.

(iii) the time-averaged aberration modes, which simulates common optical ocular aberrations [22] described by the Zernike polynomials including Zernike coma COM_{avg} (Z_3^1/Z_3^{-1}), Zernike astigmatism AST_{avg} (Z_2^2/Z_2^{-2}) and Zernike spherical aberration SA_{avg} (Z_4^0).

For each optical condition, the subject's aberrations were corrected with the adaptive optics system and the aberration generated graphically. For the native aberration condition, each individual Zernike aberrations up to the 5th order were used to generate the aberrated stimulus measured, at the exception of the Zernike defocus set to zero. All the time-averaged aberration patterns were scaled to a quarter of wavelength root-mean-square (RMS) wavefront errors. For each time-averaged aberrations tested, the dynamic sequence, which comprised fifteen frames of 33 ms, underwent an optical perturbation Δn, whose temporal position and spatial pattern was digitally controlled using an interpolated blur. The interpolated blurs, obtained from Zernike defocus (Z_2^0), Zernike astigmatism (Z_2^2/Z_2^{-2}) and Zernike trefoil (Z_3^3/Z_3^{-3}) had either a rotational or directional spatial pattern, which appeared for four consecutive frames (e.g., temporal frequency = 1/133 ms = 7.5 Hz) in one of the three following temporal segments of the dynamic sequence: Δt_1=0-133 ms, Δt_2=133-266 ms and Δt_3=266-400 ms (**Fig. 1**). To ensure that the dynamic and static sequence had the same contrast across spatial frequency, we computed the optical perturbation in the optical transfer function of the time-averaged blurred image OTF_{avg} and the interpolated blur counterbalanced across the other temporal frames (see Method for details). The visual changes were quantified by the standard deviation σ of the intensity variations of the image caused by the optical perturbation.

The sequence of a stimulus trial was as follows: a black cross serving as a fixation first appears at the center of the display. It was followed by the onset of the static and dynamic face sequence of the face stimulus. The two stimulus sequences were centered one degree from the center of fixation and were randomly switched on the left and right side of the screen with a temporal offset of 50 ms. After the offset of the stimulus, a green background image was displayed, and subjects press a keyboard button to provide a response. Typically, three repeated measurements were made for each visual condition tested.

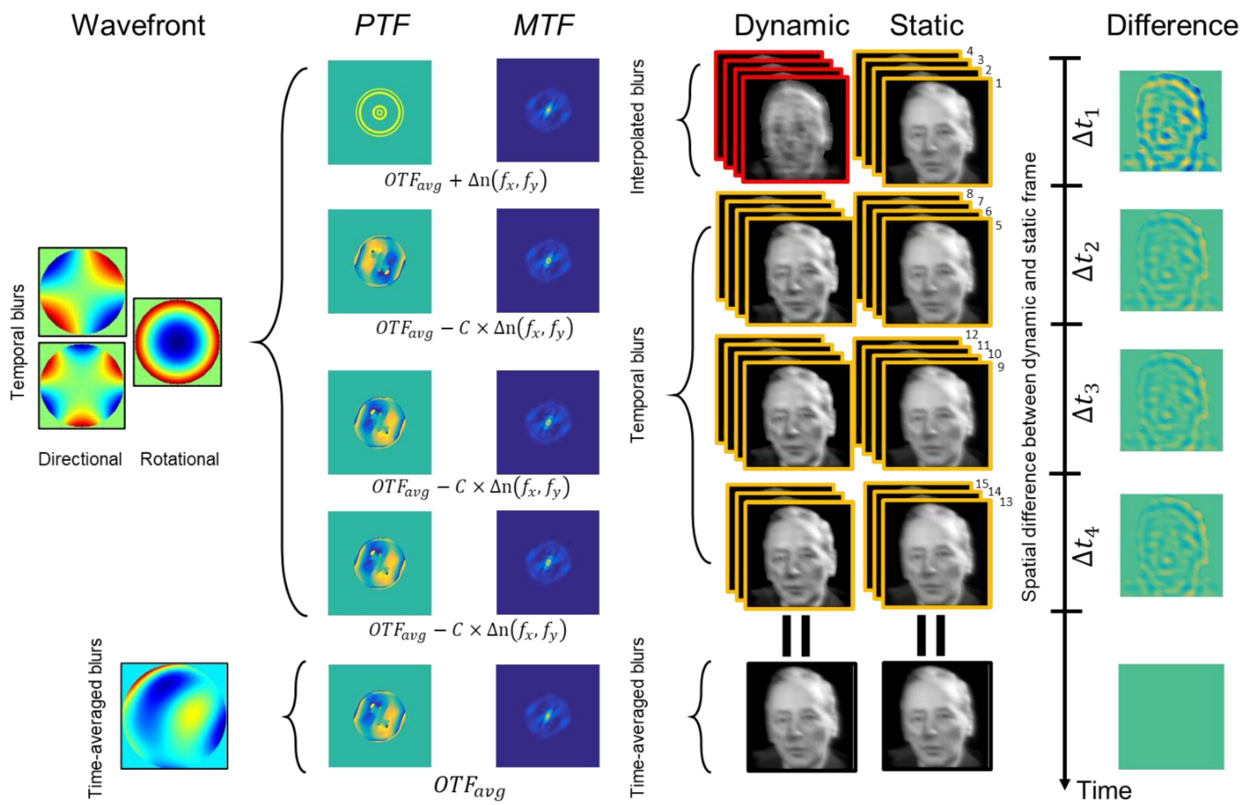

Fig. 1. Temporal sequence of the dynamic and static stimuli. Two temporal face sequence of an aberrated face with similar time-averaged optical transfer function (OTF_{avg}) are displayed side by side: one static (on the right) and the second dynamic (on the left). In the dynamic face, an optical perturbation Δn is introduced by interpolating a distinct blurred frame in one of the three first segments Δt_i of a sequence of fifteen frames. In this example, the interpolated blurred image is generated by manipulating the phase transfer function (*PTF)* of the time-averaged blur using different Zernike aberrations modes while keeping the modulation transfer function (*MTF)* same (see Methods section for details). The interpolated blur, highlighted by the red frames, is derived

from defocus Zernike and appears at the beginning of the temporal sequence for the four first frames (numbered from 1 to 4). The difference of spectra between the dynamic and time-averaged image is the largest for the interpolated blur. The dynamic face sequence averages over time such that it has the same blur OTF_{avg} as the static face sequence. Note that each phase consisted of several identical frames.

2.2 Perceptual transformation in response to interpolated blurs.

Five kinds of time-averaged blurred images (DL_{avg} , COM_{avg} , NA_{avg} , AST_{avg} , SA_{avg}) were applied an optical perturbation $\Delta n(fx, fy)^{t_1}$ at the early onset of the image Δt_1 via rotational and directional interpolated blurs. For each time-averaged blurred image, the dynamic and static face sequences with same blur on average over time were simultaneously presented. All subjects were asked to report until they perceived a change of the image in the sequence. The level of transformations introduced by the interpolated blur were classified by the subjects according to three distinct visual observations: just-noticeable variation (*JNV)*, contrast pattern variation (*CPV),* and bothersome pattern variation (*BPV)*. *JNV* was described as "the point where you first notice a change in the image, but the sharpness of the image is not changed." *CPV* was indicated as "the point at which you notice a change in the crispness and sharpness of the image pattern." *BPV* was introduced as "the point at which the optical perturbation reaches a level that cause a change in the clarity of the face stimulus". These measures require not just to report the change of interpolated blurs, but also a judgment about the effect of the interpolated blur. Such subjective measures [23-24] could be of relevance to determine the maximum amount of visual blur that can be tolerated under temporal variations without affecting the perceptual quality, that is, brought by the correction of ocular aberrations with ophthalmic lenses. The interpolated blur serving as a temporal probe produces distinct transformations of the image (**Fig. 2A**), demonstrating that blur variations at an early stage of the presentation epoch (i.e., 133 ms) can impact perception, while the blur threshold was varying systematically among three kinds of transformations. The strength of the perceived visual transformation differed across the time-averaged aberrations for all the perceived image transformations, suggesting that temporal effects are significantly affected by the time-averaged aberration. A substantial impact of temporal blurring was found for the time-averaged aberrated images as compared to the time-averaged diffraction-limited image, indicating that the average ocular aberrations do not just affect spatial perception, but could differentially alter temporal perception. Besides, our results show that the spatial symmetry of the optical perturbation (**Fig. 2B and C**) influenced the threshold of image transformation with a differential impact between the time-averaged diffraction-limited image and the time-averaged aberrated images on the relative effect of rotational and directional interpolated blurs.

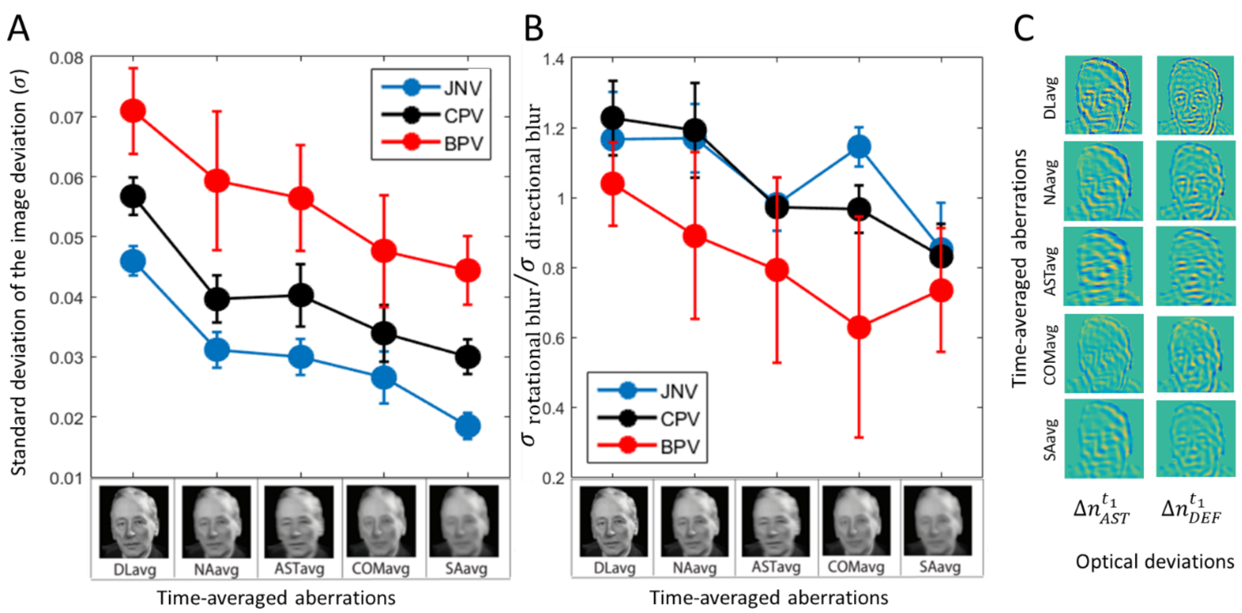

Fig. 2. Effect of temporal blurring on dynamic image changes. **A.** Average temporal blur threshold induced by interpolated blur patterns has an early temporal onset, as measured by the standard deviation of the optical perturbation Δn of the normalized images for each dynamic image changes. **B.** Average ratio between the threshold of rotational and directional blurs as a function of the time-averaged aberrations for each dynamic image changes. **C.** JNV image variations associated with the optical perturbations Δn for rotational and directional interpolated blurs as a

function of the time-averaged aberration positioned at the early time onset of the image Δt_1. Note that the higher the standard deviation, the more noticeable the temporal change caused by the interpolated blur, and the more sensitive the subjective is to changes. The data points and errors bar shows the mean value and the standard errors.

2.3 Subjective perceived sharpness with interpolated blurs.

A static and dynamic sequence with various time-averaged aberrations (DL_{avg}, NA_{avg}, AST_{avg}) were also randomly displayed. For each time-averaged aberrations, an optical perturbation appearing either at the early onset of the image Δt_1, the middle onset of the image Δt_2, or the late onset of the image Δt_3 was applied and subjects were instructed to report which image sequences appeared sharper. Due to the higher temporal frequency in the dynamic sequence, our results demonstrated that the introduction of blur to the first temporal interval (Δt_1) leads to a sharper dynamic image in comparison to the static image (**Fig. 3**). These results were consistent with the higher contrast sensitivity associated with high temporal frequencies, as compared to low temporal sinusoidal gratings [25, 26]. The interpolated blur modulates perception differentially over time with a systematic increase in image sharpness for optical perturbation having an early onset Δt_1. Conversely, tardy optical perturbation at Δt_2 and Δt_3 shows larger deviations across subjects, with the emergence of negative sharpness values (e.g., sharpness reversal) for DL_{avg} and AST_{avg}. This perceptual modulation reveals a differential processing of temporal blur over time, consonant with a change in processing over time [27]. This suggests that the sharpness of time-averaged images can be influenced by changes in the temporal structure of the stimulation.

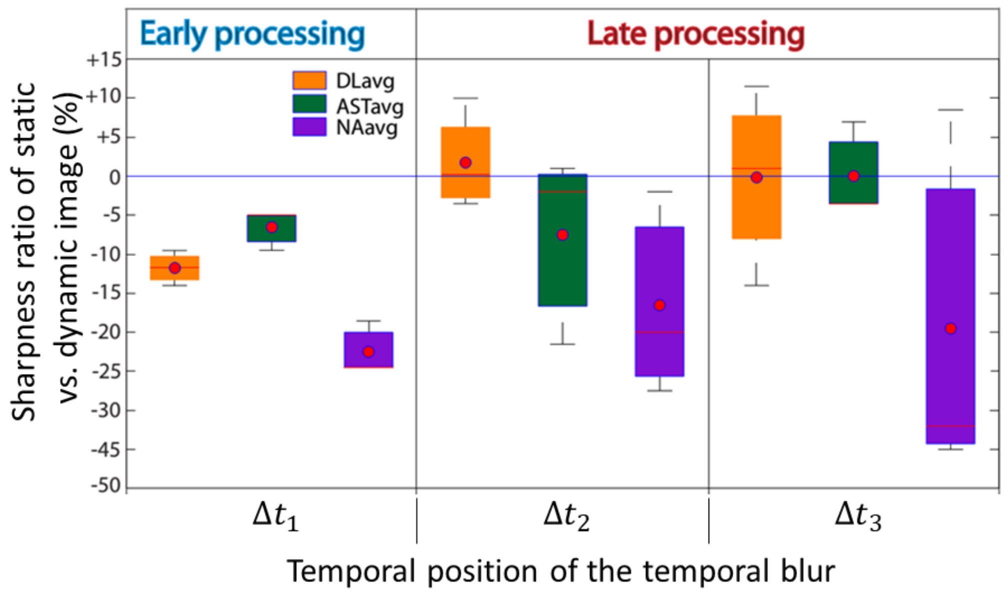

Fig.3. Effect of temporal blurring on perceived sharpness. Box plot diagram showing the level of sharpness of time-averaged aberrations for various temporal positions of the interpolated blurs Δt_1, Δt_2, and Δt_3. The baseline of 0% corresponds to the point of equality of sharpness between the static and dynamic sequences. Positive values correspond to a static image sharper than the dynamic image. The whiskers show the minimum and maximum sharpness change across subjects. The red dot indicates the mean values; the short line in boxes is the median value across subjects.

2.4 Discrimination task with interpolated blurs.

To discriminate whether the dynamic and static face sequences generate the same perception, subjects were randomly presented pair of stimuli sequence with either same or different face expressions. Visual performance was quantified by the percent of correct responses to similar pairs of faces (true-positive fraction) and incorrect response to dissimilar pairs of faces (false-positive fraction). Our results demonstrated the effect of interpolated blurs on discrimination performance for different time-averaged aberrations (**Fig. 4**), reflecting subjects may use different temporal cues to compare facial expression. Despite these individual variations, it emerged that interpolated blurs tended to cluster around different time-averaged aberrations: Clustered around the time-averaged diffraction-limited image were the most predominant among subjects, as present for all the subjects except subject S2. Clustered around other time-averaged aberrated image were also present with cluster around the time-averaged native aberration for S2 and S5 and the time-averaged spherical aberration for subject S5. It also appeared that for all the subjects except S1, the time-averaged diffraction-limited image resulted in higher true positive response (sensitivity), as compared to the time-averaged aberrated image. Overall, this suggest that discrimination performance is modulated by the time-averaged aberration with an advantage of the time-averaged diffraction-limited image under temporal blurring.

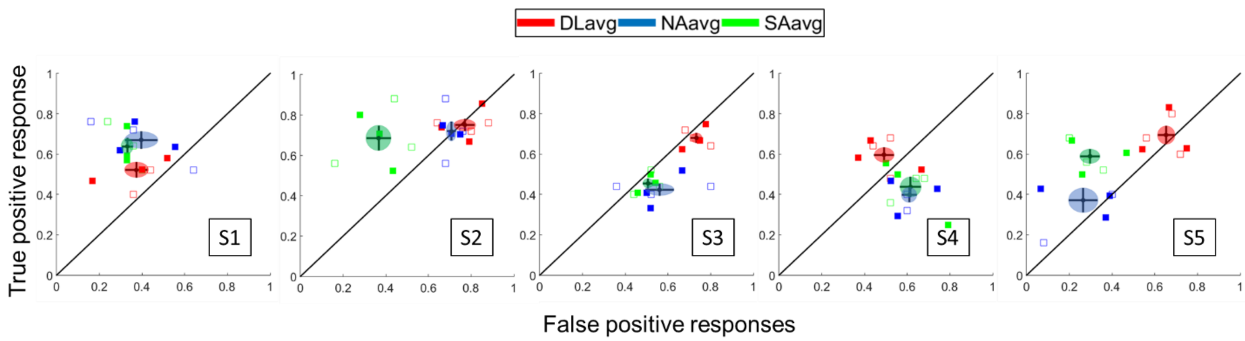

Fig.4. Effect of interpolated blurs on discrimination performance. Probability of true positive response versus false positive responses obtained for three spatial symmetries (open square symbol) and three temporal onsets (filled square symbol) of the interpolated blurs for five different subjects. Each ellipse corresponds to the receiver operating characteristic (ROC) value of a different time-averaged aberrations, including SA_{avg} (in green), NA_{avg} (in blue), and DL_{avg} (in red). Ellipses are centered on mean values, the width and height correspond to error bar of +/-1 standard error.

3. Discussion

The oculomotor dynamics causes temporal changes that remodel the spatial blur set by the ophthalmic optics. Although the temporal changes could alter the neural image produced by a time-varying neural filter, the impact of interpolated blur has not been elucidated. In this context, we implemented the adaptive optics to simulate controlled-optical perturbation and test the resulting effects on perception with and without ocular aberrations. It emerged that interpolated blur, even at the early start of a stimulus, modulate the perception of spatial blur, suggesting that the information processed over time matters in the visual effect of ocular aberrations. Furthermore, ocular aberrations appeared to modulate the effects of temporal blurring. In sum, the current study demonstrate that visual sensitivity is pertaining to the control of both spatial and temporal blurs. The neural response to interpolated and spatial blurs will be investigated along with the uncovering of the development of ocular aberrations

Processing of information is made of several temporal phases along which neurons are differently sensitive to the visual properties of the stimulus [28-33]. The inability to process a given temporal information leads to inefficiencies in the visual rendering process, holding the promise to overcome the instability of the oculomotor responses and variability of the retinal stimulus. The impact of the optical perturbation on processing relies on the observer's capability to effectively process the temporal information introduced by the interpolated blur. Although few studies used pixel noise to determine the information used by observer [34-36], a lingering question remains on how the observer strategy of processing is modeled by the image quality set by their own ocular aberrations and eye dynamics. The use of optical perturbation controlling the contrast or/and phase of the transfer function provides a new tool to elucidate the blur computed by the visual system.

In this study, using a rather localized optical perturbation, we found that, for all the ocular aberrations simulated, interpolated blurs modulate the perception of spatial blur even at the early onset of the target stimulation (**Fig. 2-4**). Interpolated blurs could differentially modify perception (**Fig. 2**), producing the enhanced image interpretation (**Fig. 3**) but the reduced visual performance (**Fig. 4**) in contrast to the influences from the static spatial blur. The degrading impact of interpolated blur on visual performance stress the importance for the visual system, as well as visual enhancement aids, of minimizing temporal blurring and not just maximize the retinal image quality. An intriguing finding is that temporal modulation in perception strongly depend on the spatial blur. In general, diffraction-limited images reduced the effects of temporal blurring (**Fig. 2-4**), as compared with the time-averaged aberrated targets. Consonant with a spatial resolution benefit of correcting ocular aberration [10-12], this finding suggests an advantage to correct the ocular aberrations in individuals, minimizing the instability of the oculomotor response leading to interpolated blurs. Overall, this suggests a potential role of ocular aberration in the balance between spatial and temporal aspect of visual processes, such as resolution. The use of same/similar images can cause a repeated pattern of stimulation under stabilization of the optical images forming onto the retina. While the repetition of stimuli is likely to affect the observer's attention to details and adaptively change temporal processing, whether, and to what extent, this adaptability of processing is constrained by an individual idiosyncratic strategy and ocular aberrations remains to be determined. The ability to adapt the perturbation caused by temporal variation may have relevance for the development of training visual test aimed at reallocating the processing resources involved in temporal and spatial resolution. Given the various experimental constraints involved in psychophysical testing with adaptive optics simulator, we limited the sample size in the study in order to assess the potential effect of interpolated blur on processing. Although our results demonstrate a consistent effect of the interpolated blurs with ocular aberrations, a larger sample size study will be required to fully elucidate how the dynamic properties of blur are computed by the visual system when the temporal instabilities of the stimulation are present.

4. Methods

4.1 Subjects

A total of ten subjects (aged 30 $\pm$ 10 years old, 8 males and 2 females) from the Lab participated in the study. Each subject was free from ocular pathology and had no history of ocular surgery. Each subject gave informed consent after the protocol and possible consequences were explained to them. The research was approved by the National University of Ireland, Galway, Ethics Committee and followed the tenets of the Declaration of Helsinki. All the information was coded and strictly confidential.

4.2 Apparatus & stimuli

Measurements were performed in a dark room using a compact custom-built adaptive optics vision simulator (**Fig. 5**) [37]. The visual simulator was inspired by a previous version used for simulating the effect of higher-order aberrations [38-39].

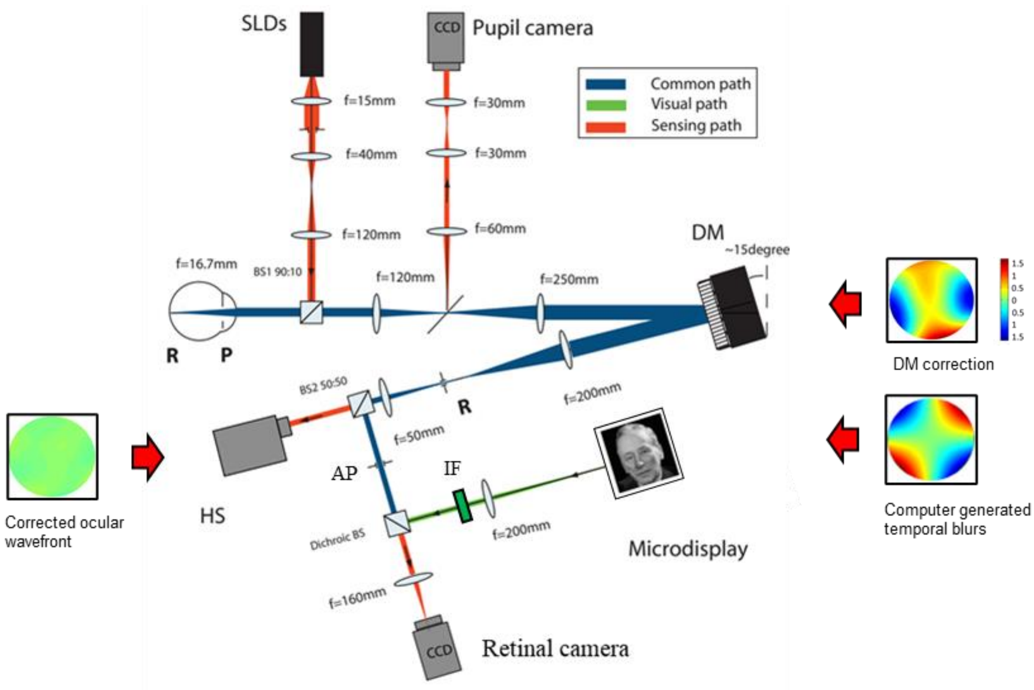

Fig. 5 Schematic diagram of the adaptive optics system used. The infrared light (836 nm+/-40 nm, in red) was used for measuring the wavefront aberration and driving the deformable mirror, in contrast to the visual experimental path in green. The overlapping of measuring and visual paths was indicated in blue. The dynamic and static face sequence were computer-generated and digitally rendered via the microdisplay while the deformable mirror corrected the ocular aberrations of the subject measured in real-time via the Hartmann-Shack. DM, deformable mirror; HS, Hartmann-Shack; SLD, super-luminescent source; CCD, charged-coupled device camera; AP, artificial pupil; IF, interference filter, P & R, pupil and retinal conjugates.

The visual simulator consists of an illumination arm, a pupil monitoring branch, a wavefront sensing and correction, and a visual branch. The illumination arm projected an infrared illumination beacon (836 nm) from a superluminescent diode (Superlum, Ireland) onto the cornea. Light focusing onto the retina was then directed onto the wavefront sensing arm, which conjugates the pupil of the eye with a Hartmann-Shack wavefront sensor (HASO 32, Imagine Eyes, France), an electromagnetic deformable mirror (MIRAO 52e, Imagine Eyes, France), a pupil camera and a retinal camera. Throughout the tests, the pupil camera was used to stabilize the subject's position, which was controlled via a chinrest fixed onto a 3-D translation stage. Once ocular aberrations were measured by the Hartmann-Shack wavefront sensor, defocus was corrected by a Badal optometer and the subject's natural ocular aberrations (at the exception of tip and tilt) were corrected in a closed-loop adaptive operation using the deformable mirror. A typical closed-loop correction provided a correction down to a level of about 0.1μm root-mean-square (RMS) wavefront errors over a pupil of 5mm diameter, at a frame rate of about 15 Hz. The adaptive correction enables to emulate the effect of higher-order aberration on high-resolution images via the use of a large pupil. During the adaptive optics correction, visual stimuli were produced on a compact OLED microdisplay (600 x 800 pixels, eMagin) and filtered using an interference filter (wavelength: 550 nm $\pm$ 50 nm) so as to prevent chromatic aberrations. To limit the non-common path aberrations, the monochromatic stimuli were projected to the retina through the visual branch using two optical elements only, including a lens and a beam-splitter. Stimuli were seen at optical infinity through a circular artificial pupil (diameter: 5mm), conjugated to the eye pupil. The visual stimuli were generated using PsychoToolbox routines in MATLAB software [40].

4.3 Spatial Stimuli

A high contrast human face was chosen as the visual stimulus in reason of the high level of cognitive processing involved in the analysis of human faces [41-43], making it relevant to study temporal processes spanning over the scale of hundreds of milliseconds. It is also one of the most common social stimuli, and its broad spatial frequency composition [44] is of relevance to understanding the way information is processed for complex images (e.g., with a wide range of spatial frequencies and orientations) present in the real-world stimulation. The photo of human face was utilized to create dynamic and static image sequences, with the same time-averaged optical transfer function for the two sequences. The stimulus of each image sequence was presented at optical infinity and subtended about 40 arcmin onto the retina, respectively. The view of face results in a long-lasting response of event-related brain potentials (with a late negativity peak decaying above a latency of 350ms [45]). The total number of each image sequence was set to fifteen frames to allow sufficient time exposure for fully processing the details of the image. The time-averaged stimulus was graphically generated by convolution of the original image with a point spread function for the 5mm pupil diameter, given the monochromatic light source with a wavelength of 550 nm. Given that the range of spatiotemporal blur manipulation using adaptive element remains restricted, this method provided the most optimal solution to present images having a spatiotemporally varying blur structure.

4.4 Interpolated blur

The interpolation produced optical perturbation between consecutive frames at a given time t_i. The optical perturbation $\Delta n(fx, fy)^{t_i}$ was computed in the optical transfer function of the time-averaged blurred image $OTF_{avg}(f_x, f_y)$, as follows:

$$\Delta n\left(f_x, f_y\right)^{t_i} = OTF_{temp}\left(f_x, f_y\right) - OTF_{avg}(f_x, f_y), \text{ (Equation 1)}$$

where $OTF_{temp}\left(f_x, f_y\right)$ is the OTF of the interpolated blurred image at the given time Δt_i. Both rotational and directional interpolated blurs were simulated (**Fig. 1**). In the simulation, rotational interpolated blurs were obtained from Zernike defocus (Z_2^0), whereas directional blurs were obtained from Zernike astigmatism (Z_2^2/Z_2^{-2}) and Zernike trefoil (Z_3^3/Z_3^{-3}).

The OTF of the interpolated blurred image was computed as:

$$OTF_{temp} = MTF \times exp\ (i \times PTF_{temp}), \text{ (Equation 2)}$$

with the phase transfer function of the OTF_{temp}:

$$PTF_{temp} = (Im(OTF)/Re(OTF)\ , \text{ (Equation 3)}$$

and the modulation transfer function (MTF) of the time-averaged or the temporal blur.

$$MTF = \sqrt{(Re(OTF)^2 + Im(OTF)^2)}. \quad \text{(Equation 4)}$$

To warranty the dynamic sequence sharing the same average OTF over time with static sequence, we compensated the spatial perturbation using a demodulation $\Delta n'(f_x, f_y) = -C \times \Delta n(f_x, f_y)$ in each frame of the three remaining temporal phases (**Fig. 1**), where the constant

$$C = \frac{number\ of\ frame\ of\ the\ interpolated\ blur}{(total\ number\ of\ frame - number\ of\ frame\ of\ the\ interpolated\ blur)} = 0.3636, \quad \text{(Equation 5)}$$

In contrast to other frames, the interpolated frame carried more aberration. Various strategies are possible for the perturbation proposed. Given the temporal resolution of the visual system, a restricted number of frames was necessary to make the target and optical perturbation perceived as part of the same unitary pattern, and therefore prevent the observer to disentangle the perturbation from the actual target. To provide sufficient sensitivity to the temporal information, we chose four frames with the temporal frequency of 7.5 Hz of the interpolated blur [25].

4.5 Psychophysical procedure:

4.5.1 *perceptual transformation in response to temporal blurs.*

Eight participants were selected to report the influence of an optical perturbation $\Delta n(fx, fy)^{t_1}$ introduced at the early onset of the image Δt_1 on the transformation of time-averaged blurred images (DL_{avg}, COM_{avg}, NA_{avg} , AST_{avg}, SA_{avg}) . We anticipated that the early perturbation would be more difficult to disentangle from the actual target, and thus lead to a stronger disruption of processing, in accordance with the larger impact observed for early variation occurring near the onset of a target, as compared to late ones [20]. In this context, we chose an early temporal onset of the temporal blur to maximize the effect of the optical perturbation. For each pair of face stimuli, subjects were asked to report by pressing a keyboard button until a first change was observed in the sequence. After each button press, a new dynamic image sequence was displayed in comparison with the static blurred image, used as a reference. To determine the optical perturbation threshold for which the time-averaged image appear to change, subjects were allowed to modulate the magnitude of the optical perturbation of the dynamic sequence back and forth before reporting a response via a press button. After the determination of the first image transformation, subjects were instructed to increase the magnitude of the interpolated blur again until they could perceive a new change in the perceived image, and so on.

4.5.2 Subjective perceived sharpness with interpolated blurs.

Four participants were selected to report the influence of the temporal position of the optical perturbation on subjective perceived sharpness of time-averaged blurred images (DL_{avg}, NA_{avg} , AST_{avg}) . For each time-averaged aberration, 200 trials were performed within a single run, where three interpolated blurs were randomly tested: the optical perturbation $\Delta n(fx, fy)^{t_1}$ introduced at the early onset of the image Δt_1, $\Delta n(fx, fy)^{t_2}$ introduced at the middle onset of the image Δt_2, and $\Delta n(fx, fy)^{t_3}$ introduced at the late onset of the image Δt_3. This temporal partition intended to compare the effect of the early optical perturbation at Δt_1, occurring in the first millisecond of the stimulus onset (i.e., <133 ms), from the later optical perturbation Δt_2 and Δt_3, expected to affect neural filtering at a later attentive stage [46]. Note that the optical perturbation was not introduced in the Δt_4 period corresponding to a late attentive stage to prevent the observer to disentangle the optical perturbation from the actual target. All the temporal position of the optical perturbation were randomly distributed during a run over 200 trials. Using a two-alternative forced-choice task procedure, the subject's task was instructed to compare the dynamic and the static face sequence by reporting the sharper image for each ocular aberration.

4.5.3 Discrimination task with interpolated blurs.

Five participants were selected to report the influence of the temporal position and spatial pattern of the optical perturbation on visual performance of time-averaged blurred images (DL_{avg}, NA_{avg} , AST_{avg}). For each time-averaged blurred images, 150 trials were presented in a single run: in half of the trial, the subjects were presented the same static face sequence and, in the other half, two distinct versions of the original face were generated for the static and dynamic sequence, so that the face exhibit a distinct expression. As in the second experiment, three distinct temporal onsets of the spatial perturbation ($\Delta n(fx, fy)^{t_1}$, $\Delta n(fx, fy)^{t_2}$, $\Delta n(fx, fy)^{t_3}$) were randomly tested. For each temporal pattern, three distinct interpolated blurs were presented, derived from Zernike defocus, Zernike astigmatism and Zernike trefoil. In a two-alternative forced-choice task, the subject was asked to discriminate whether the dynamic and the static face sequence were having the same expression or not. For each spatial symmetry and time positions of the optical perturbation, visual performance was quantified by the percent of correct responses to similar pairs of faces and incorrect response to dissimilar pairs of faces, i.e. the percent of true-positive responses and false-positive responses. Measurements were then analyzed based on the receiver operating characteristic (ROC) (**Fig. 4**) [47]. For each viewing condition, a *ROC* value was obtained, which represented the true-positive fraction (sensitivity) versus false-positive fraction (specificity). The characteristic of the subject's temporal response is given by the trade-off between sensitivity and specificity under a given blur.

Disclosures

Competing Interests: The authors declare no competing financial interests.

References

1. R. Desimone, J. Duncan, Annu. Rev. Neurosci. **18**,193 (1995)
2. A.B. Watson, A.J. Ahumada, J. Vis. **8**,17 (2008)
3. J. Kulikowski, D. Tolhurst, J. Physiol. **232,** (1973)
4. G.E. Legge, Vis. Res.**18**, 69 (1978)
5. V.P. Ferrera, T.A. Nealey, J.H. Maunsell, Nature **358**, 756 (1992)

6. A.M. Derrington, J. Krauskopf, P. Lennie, J. Physiol. **357**:241(1984)

7. J.J. McAnany, K.R. Alexander, Vis. Res. **46**:1574 (2006)

8. J. Hegdé, Prog. Neurobiol. **84**, 405 (2008)

9. E.A. Allen, R.D. Freeman, J. Neurosci. **26**, 11763 (2006)

10. J. Liang, D.R. Williams, D.T. Miller, J. Opt. Soc. Am. A **14**, 2884 (1997)

11. D. Williams, G-Y. Yoon, J. Porter, A. Guirao, H. Hofer, I. Cox, J. Refract. Surg. **16** ,S554 (2000)

12. G-Y. Yoon, D.R. Williams, J. Opt. Soc. Am. A **19**, 266 (2002)

13. E.A. Rossi, A. Roorda, J. Vis. **10**:11 (2010)

14. A. Ravikumar, E.J. Sarver, R.A. Applegate, J. Vis. **12**:11(2012)

15. C-C .Chang, A. Chu, S. Meyer, Y. Ding, M.M. Sun, P. Abiri, K.I. Baek, V. Gudapati, X. Ding, P. Guihard. Theranostics.**11**:1162 (2021)

16. E. De Lestrange-Anginieur, C-s. Kee, PLoS One **15**, e0234380 (2020)

17. E. De Lestrange-Anginieur, T. Leung, C. Kee, Vis. Res. **185**, 88 (2021)

18. L. Sawides, C. Dorronsoro, A.M. Haun, E. Peli, S. Marcos, PLoS One **8**, e70856 (2013)

19. A. Radhakrishnan, L. Sawides, C. Dorronsoro, E. Peli, S. Marcos, J. Vis. **15**,15 (2015)

20. P. Neri, DJ. Heeger, Nat. Neurosci. **5**, 812(2002)

21. P. Neri, DM. Levi, J. Neurophysiol. **97**, 951(2007)

22. L. Chen, B. Singer, A. Guirao, J. Porter, D.R. Williams, Optom. Vis.Sci. **82**, 358 (2005)

23. K.J. Ciuffreda, A. Selenow, B. Wang, B. Vasudevan, G. Zikos, SR. Ali, Vis. Res. **46**, 895 (2006)

24. E. De Lestrange-Anginieur, CS. Kee, Heliyon **6**, e04153 (2020)

25. J.G. Robson, J. Opt. Soc. Am. A **56**, 1141 (1966)

26. Jr. LE. Arend, Vis. Res. **16**, 311 (1976)

27. V. Goffaux, J. Peters, J. Haubrechts, C. Schiltz, B. Jansma, R. Goebel, Cereb. Cortex. **21**, 467 (2011)

28. D.L. Ringach, M.J. Hawken, R. Shapley, *Nature*.**15**, 281(1997)

29. C.E. Bredfeldt, D.L. Ringach J. Neurosci. **22**,1976 (2002)

30. Mazer J.A., Vinje W.E., McDermott J., Schiller P.H. & Gallant J.L. Proc. Natl Acad. Sci. **99**, 1645 (2002)

31. D.L. Ringach, M.J. Hawken & R. Shapley, J.Neurophysiol. **90**, 342 (2003)

32 M.D. Menz & R.D. Freeman, J. Neurophysiol. **91**, 1782(2004)

33. M. Volgushev, T.R. Vidyasagar & X. Pei, Vis. Neurosci. **12**, 621 (1995)

34. C.K. Abbey, M.P. Eckstein, Front. Psychol. **5**, 345 (2014)

35. J.M.Gold, Front. Psychol. **5**,142 (2014)

36. CP. Taylor, P.J. Bennett, A.B. Sekuler. Front. Psychol. **5**, 578 (2014)

37. H. Guo, E. DeLestrange, J. Biom. Opt. **20**, 036008 (2015)

38. K.M. Hampson, I. Munro, C. Paterson, C. Dainty. J. Opt. Soc. Am. A **22**,1241 (2005)

39 E. Dalimier, C. Dainty, J.L. Barbur J. Mod. Opt. **55**, 791(2008)

40. D.H. Brainard Spat. Vis.**10**,433 (1997)

41. W. Luo, W. Feng, W. He, N-Y. Wang, Y-J. Luo, NeuroImage. **49**,1857 (2010)

42. M. Xia, X. Li, C. Ye, H. Li, Adv. Psychol. Sci. **22**,1556 (2014)

43. S. Schindler, F. Bublatzky, Cortex. **130**, 362 (2020)

44. P. Vuilleumier, J.L. Armony, J. Driver, R.J. Dolan. Nat. Neurosci. **6**,624 (2003)

45. T.F. Münte, M. Brack, O. Grootheer, B.M. Wieringa, M. Matzke , S. Johannes, Neurosci. Res. **30**, 25 (1998)

46. V.A. Lamme, P.R. Roelfsema, Trends Neurosci. **23**, 571 (2000)

47. C.E. Metz, Semin. Nucl. Med. **8**, 283 (1978)